Fusion Engineering and Design 186 (2023) 113353

Contents lists available at ScienceDirect

Fusion Engineering and Design

journal homepage: www.elsevier.com/locate/fusengdes

Failure analysis of a heavy gauge fastener of the ITER toroidal field gravity support system

Stefano Sgobba [a,*], Ignacio Aviles Santillana [a], Katie Elizabeth Buchanan [a], Michal Dalemir Celuch [a], Mickaël Crouvizier [a], Ana Teresa Perez Fontenla [a], Enrique Rodriguez Castro [a,b], Cornelis Beemsterboer [c], Min Liao [c], Thierry Schild [c], Shiqiang Han [c], John-Morgan Coulet [d]

[a] CERN, CH-1211 Genève Switzerland
[b] University Carlos III of Madrid, Campus Leganes, Av. Universidad 30, 28911 Madrid Spain
[c] ITER Organization, 13067 Saint Paul Lez Durance Cedex France
[d] Framatome - IBPER-F Department - CNPE Consortium - ITER Project TAC1, Route de Vinon sur Verdon, CS 90 046 - 13067, St. Paul lez Durance Cedex, France

ARTICLE INFO

Keywords:
ITER toroidal field
Gravity support
Nickel base superalloys
Delayed failure

ABSTRACT

The Gravity Supports (GS) of the ITER Toroidal Field (TF) coils are positioned at the bottom of the machine and are situated under the 18 toroidal field coils. Each support includes 26 high strength bolts with M60 and M85 gauge. The TFGS will sustain a total load of about 11,000 tonnes of dead weight of the magnet system. Moreover, they will be exposed in operation to large electromagnetic forces and possible seismic dynamic loads. The bolts are manufactured from forged rods of double aged UNS N07718 (also known as Inconel® 718), a high strength nickel base superalloy. Stringent material specification and quality controls requirements apply to the threaded bolts and the other components of the GS. A complete break of one M85 bolt was discovered, that occurred about 40 days after its installation and preloading, prior to the application of any operating stress. Half of the part blew out from the bolthole and was found lying horizontally on the GS top area. Following the incident, a comprehensive failure analysis was carried out, based on a combination of non-destructive and destructive examinations including advanced techniques such as computed microtomography, immersion ultrasonic testing (UT) and fracture mechanics. The delayed rupture was understood as due to a combination of cavities not closed by the forging operations associated to a continuous network of brittle secondary phases at the grain boundaries, resulting in a local lack of ductility, poor impact toughness and mechanical properties locally lower than specified. As a consequence of the incident, UT procedures were developed to confirm that the remaining bolts, including the installed ones, are free of cavities using sufficiently conservative criteria and fit for purpose prior to operation. In particular, in-situ axial inspections allowed installed bolts that could contain relevant imperfections to be identified and replaced.

1. Introduction

The 18 Gravity Supports (GS) of the ITER Toroidal Field (TF) coils are installed on the cryostat base matching the edge of each TF coil. They will sustain 11,000 tonnes of dead weight while having sufficient compliance to adapt to the movement of the coils in the different phases of cooldown. In operation, they will be exposed to large electromagnetic forces and possible seismic loads [1]. The bottom of TFGS is fixed to the cryostat base through 26 high strength fasteners, namely heavy gauge M60 and M85 threaded bolts issued from forged rods of UNS N07718 (also known as Inconel® 718). UNS N07718 is a high strength nickel base superalloy, submitted to a double ageing treatment, following the ASTM A1014 requirements, that confers to the alloy the proper combination of high strength and stress-rupture ductility, including at cryogenic temperature [2]. Composition limits are also per ASTM A1014 with additional restrictions for Co ($\leq$ 0.01%) and Ta ($\leq$ 0.05%). The components of the TFGS interface at the top with the TF coil, operating at 4 K, while the bottom is at approximately Room Temperature (RT). The material was produced based on a stringent specification. The melting and remelting practices, the composition and the whole

* Corresponding author.
E-mail address: Stefano.Sgobba@cern.ch (S. Sgobba).

https://doi.org/10.1016/j.fusengdes.2022.113353
Received 30 September 2022; Received in revised form 7 November 2022; Accepted 19 November 2022
Available online 26 November 2022

production process including the thermal treatments should result in products featuring high strength, ductility and toughness (at RT yield strength $Rp_{0.2} > 1035$ MPa, tensile strength Rm > 1275 MPa, elongation at breakdown $A > 12\%$, reduction of area $Z > 15\%$; at 4 K $Rp_{0.2} > 1350$ MPa, Rm > 1600 MPa, $A > 8\%$, $K_{IC} > 75$ MPa$\sqrt{m}$ in LR orientation - load applied along the longitudinal direction and crack propagating along the radial direction). High cleanliness is specified (non-metallic inclusions following ASTM E45 method D are limited to at most 2 for inclusion types A, B, C and D). Macroinclusions are not permitted. The microstructure shall be free of freckles, white spots and Laves phases. Moreover, binding specifications apply to grain size and homogeneity of microstructure (average grain size number $G = 5$ or finer as defined in ASTM E112 and homogeneous within the range of ± 1 around the true average value). Consistently, the steelmaking route is imposed by specification as Vacuum Induction Melting (VIM) followed by Vacuum Arc Remelting (VAR), while allowing possible further remelting by VAR or Electroslag Remelting (ESR).

Despite the stringent requirements and the extensive quality controls applied to the forged prematerial and to the bolts, a complete break of one M85 bolt was discovered, that occurred about 40 days after its installation and preloading up to 2.65 MN (45.1% of $Rp_{0.2}$), prior to the application of any operating stress. The upper half of the part blew out from the bolthole and was found lying horizontally on the Cryostat Base near the TFGS (Fig. 1) while the lower half part shot downward and lied in the confined space of Cryostat Base. The present paper reports the results of the comprehensive failure analysis carried out following the incident.

2. Product investigated and inspections applied

All the bolts were issued from bars forged with a reduction of at least 7, following a two step preheating of the billets (800~850 °C for at least 2 h and 1150 °C for at least 1.5 h). Based on mill certification (properties were assessed per lot by sampling on extra lengths of the forged bars), the chemical composition (Table 1), the fabrication route, the heat treatment, the mechanical properties and the microstructure (G and inclusion content) were according to specification, with the exception of the steelmaking route which has been VIM+ESR in place of specified VIM+VAR, featuring similar attributes [3]. The bars were examined by Ultrasonic Testing (UT) in accordance with ASME Section V, Article 5, while the examination procedure and acceptance standard were in

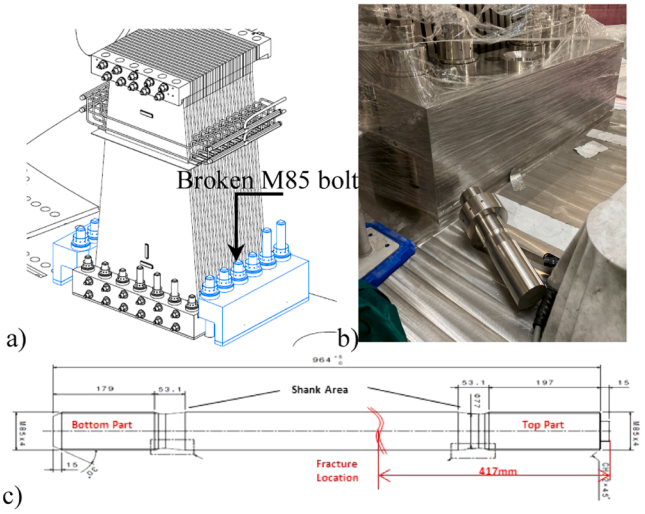

Fig. 1. a) Complete GS, including M60 and M85 bolts. b) Top part of the broken bolt that blew out from the bolthole. The delayed catastrophic failure occurred near the bottom of an L – shape clamp of the TFGS18, visible on the back. c) Rupture occurred in a full section of the stud, outside the reduced diametre shank areas.

Table 1
Applied manufacturing route and chemical composition (product analysis).

Product identification	Manufacturing route	Reduction ratio	Chemical composition (heat analyses,% by mass, balance Fe)															
			C	Mn	Si	P	S	Cr	Ni	Mo	Ta	Ti	Al	Co	B	Cu	Nb+Ta
M85 bolt	VIM + ESR +Forging	> 7	0.054	0.20	0.21	0.003	0.002	19.02	53.68	3.27	0.012	0.73	0.63	0.010	0.0012	0.049	5.33
Specification requirements	*VIM+VAR, VIM+VAR+ESR or VIM+VAR+VAR*	*> 7*	*<0.08*	*<0.35*	*<0.35*	*<0.015*	*<0.015*	*17.0–21.0*	*50.0–55.0*	*2.80–3.30*	*0.05*	*0.65–1.15*	*0.20–0.80*	*<0.10*	*<0.006*	*<0.30*	*4.75–5.50*

accordance with ASME Section III, NB-2542. Based on the above standards, the acceptance criteria was with reference to a Flat Bottom Hole (FBH) of 8 mm diametre.

UT on the inspectable portions of the broken stud (and for reference on fully comparable products issued from the same lot or production route) was performed by both contact and immersion tests in radial and axial direction with a Technisonic Triton 1000 system and probes up to 5 MHz, allowing a calibration on Side Drilled Holes (SDH) as fine as ∅1.6 mm. Framatome-Intercontrôle performed additional UT immersion tests with similar resolution and reference to SDH and FBH of ∅ 1.5 mm. Further details about the UT inspections and about the measures taken to inspect the remaining bolts, including the installed ones, in order to verify that they are fit for purpose prior to operation, are provided in [4]. Complementary X-ray micro-tomography (CT) investigations in volumes of interest were performed at CERN with the help of a ZEISS METROTOM 1500 tomograph. The achieved resolution (voxel size) is in the order of 130 μm. Moreover, metrological inspections were performed through a 3D optical scanner (MetraSCAN® from Creaform), with a 25 μm resolution.

Metallurgical observations were carried out with the help of a Zeiss AxioImager microscope and Keyence VHX-7000 and VHX-6000 Digital Microscopes (DM). SEM and FIB-SEM observations were performed respectively with Zeiss Sigma and Sigma 500 Field Emission Gun (FEG) systems, and a Zeiss XB540 FIB-SEM unit. Secondary Electrons (SE), Backscattered Electrons (BSE) modes and Energy dispersive X-ray Spectroscopy (EDS) were applied in order to identify and analyse the secondary phase distribution and their nature. These phases were crystallographically confirmed by X-ray Diffraction (XRD) through a fully equipped D8 Discover Plus system by Bruker.

Tensile tests were performed according to ASTM E8M method C (crosshead speed controlled at 0.015±0.03 min^{-1}, with a preload of 3 MPa). Fracture mechanics tests were performed according to ISO 12135 on specimens extracted in L-R orientation that is the most representative of the observed failure of the broken stud. Specimens for impact toughness tests were machined according to ISO 148–1, with the notch (featuring a depth of 2 mm) in G position (crack propagation in the radial – circumferential plane, also representative of the failure). Finally, Brinell hardness was measured per ASTM E10 through a "Type a" device. Values are checked against requirements of ASTM B637 (HB > 331) and of the specification (331 HB - 444 HB).

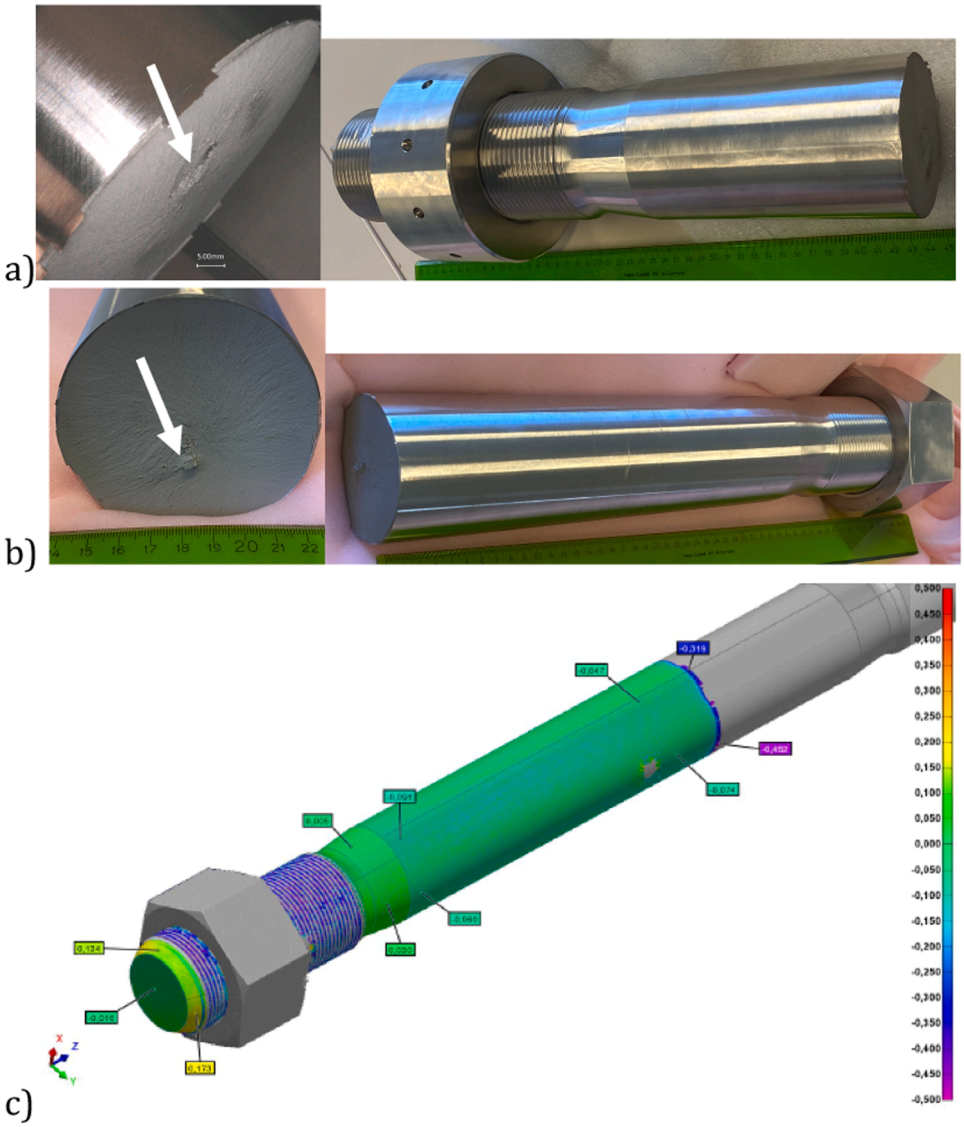

Fig. 2. Fracture surfaces of the broken stud (the initiation site is identified by a white arrow). a) top portion; b) bottom portion; c) dimensional metrology (top portion shown) concludes on almost total absence of necking.

3. Failure analysis

Fig. 2 illustrates the appearance of the two fracture surfaces of the broken stud. The macroscopic observations confirm a very flat fracture and almost total absence of shear lips.

This is distinctive of limited ductility and is unexpected for this alloy, usually featuring cup-and-cone ductile fracture when broken by tensile overload [5]. Dimensional metrology (Fig. 2c) confirms absence of significant necking (< 1 mm diametric reduction, corresponding to $Z < 2\%$, far below the minimum specified value of 15%). The initiation site is easily identified in the bulk, where all the river patterns converge. It spans over several tens of mm^2. It is slightly eccentric from the axis and far from the free surface, hence excluding a bending moment that would have occurred in operation due to misalignment or off-axis loading. Curved radial lines emanate from the eccentric initiation site and eventually propagate in a radial manner. SEM observations of the fracture surfaces (Fig. 3a) show a generalized quasicleavage, intergranular secondary cracks and interconnected networks of fractured precipitates. They reveal smooth surfaces and surface terraces, evidencing a preexisting local lack of cohesion. Some surfaces at the initation site show a solidification structure, pointing to cavities not closed by the forging reduction. Similar cavities were identified in the vicinity of the fracture surface by immersion UT and confirmed by CT and metallographic observations. In particular, some 10 mm upstream of the top fracture surface, a cavity was identified in the bulk at a radial distance of ~ 8 mm from the axis, in a matching position with respect to the one of the initiation site (Fig. 4).

Grain structure is fine and equiaxis, with G spanning from 7 in the centre to 9 at the periphery of the stud, within the specified limits. However, GB decoration is widely observed (Fig. 3c), under the form of continuous networks of secondary phases along GB. The aspect of these precipitates is compatible with intermixed acicular δ–phase and Laves' phase (platelets). EDS analyses and XRD confirm δ–phase (Ni_3Nb) and presence of Laves (Fe_2Nb crystal structure, enriched in Mo), whose composition assessed by EDS (30.6Ni14.3Fe13.1Cr-12.2Mo14.3Nb) is compatible with the predicted one [6]. Isolated carbides (NbC) are also observed. The excessive presence of δ–phase at the GB is understood as due to the high Nb content of the alloy (over 5.3%), towards the high bound allowed by standards in force (5.50%), promoting GB precipitation when submitted to the standard ASTM A1014 heat treatment.

In order to exclude hydrogen embrittlement as a possible cause of the delayed rupture, its content at the ppm level was assessed by Instrumented Gas Analyses (IGA), together with O and N content. The H content of the broken stud ranges from 1.02 ppm close to the inititation of the rupture to 1.11 ppm close to the outer surface. These values are even lower than expected for the baseline concentrations (2–3 ppm) for this alloy [7]. In order to measure an effect on ductility, the content should be in the tens of ppm range [8]. To be noted that the stud has never been exposed to a H atmosphere or H charging. On the other hand, the measured N content (93 to 108 ppm) is well above baseline concentration expected for wrought products of the alloy (60 – 80 ppm) and might be critical since excessive N may contribute to form microporosity by promoting TiN formation that affect, in combination with carbides, the liquid feeding of the interdendritic regions during solidification [9].

In order to check the compliance of the mechanical properties of the stud in the available volumes adjacent to the failure, tensile tests were performed on six specimens extracted with their axis parallel to the stud axis from three radial locations, namely inner diameter, half radius and 3/4 radius (Table 2). $Rp_{0.2}$ is well under the specified value (1035 MPa), in all positions but particularly in the core of the stud where Rm is also under specification value. To be noted the very poor ductility of the core of the product with A values as low as 3.1% for min. 12% specified. All specimens exhibit a flat fracture surface, with absence of localized necking. In addition to these specimens, four specimens for fracture mechanics tests were extracted, one from the innermost radial position and three at approximately mid-radius of the stud. The spread of fracture

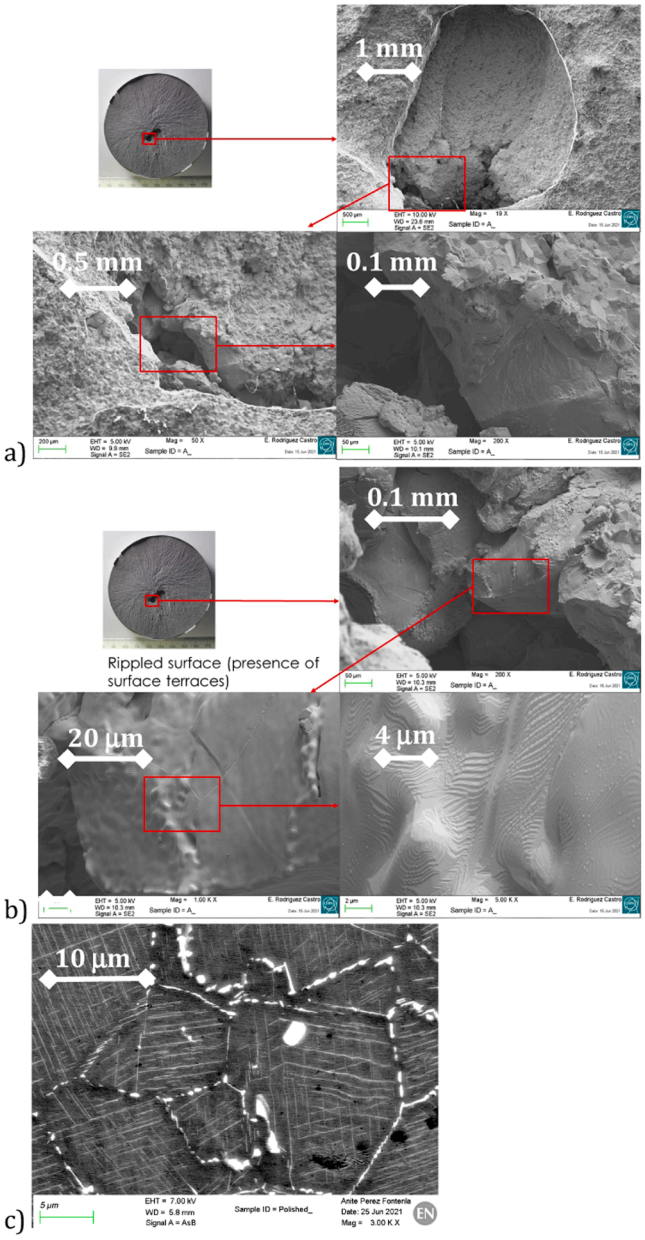

Fig. 3. SEM observations of the initiation site. a,b) A system of cavities in the continuity of the inititation event showing rippled surfaces is observed in the bulk of the stud; c) The Grain Boundaries (GB) are affected by an extensive precipitation of secondary phases.

toughness with respect to the radial position of the crack is rather limited: 66.1 ± 3.7 $MPa\sqrt{m}$. Three impact toughness specimens were also extracted and tested with very limited spread of results (10.3 ± 0.5 J, corresponding to 12.9 ± 0.6 J/cm^2).

Nonetheless, these values are extremely poor if compared to minimum requirements of standards in force such as API 6A718, requiring a minimum average (individual) value of 47 (41) J for this alloy, specially treated to avoid the observed continuous networks of secondary phases along GB, that are detrimental and would be unacceptable to the above standard. Standard EN 10269 covering the use of this alloy for application to fasteners is less severe and imposes a min. of 12 J, also not achieved. Hardness profiles (from the surface to the core of the products) have been measured on one cross section along two radii (Table 3). The sample is softer towards the core. All measured values are within the specified range (331 HB - 444 HB) and not far from the value reported in the certification of the stud (413 HB).

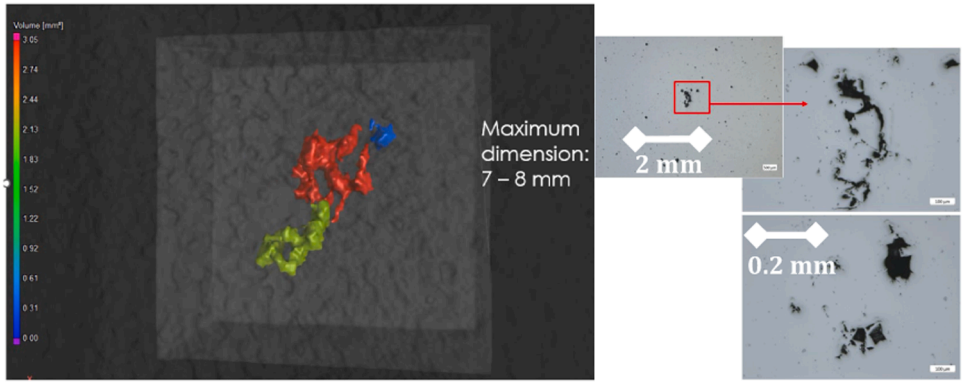

Fig. 4. Typical cavities as confirmed by CT (left) and microoptical observation (right) in the volume of material surrounding the breakdown.

Table 2
Tensile properties in the vicinity of the failure. Red values do not comply with the requirements of the technical specification.

	Tensile	$R_{P0.2}$ [MPa] Req ≥ 1035 MPa	R_M [MPa] Req ≥ 1275 MPa	A [%] Req ≥ 12%
Inner	Specimen 2	883.1	1174.1	3.09
	Specimen 4	856.4	1164.8	4.25
Mid	Specimen 5	878.0	1298.8	13.2
	Specimen 6	999.3	1316.5	9.40
Outer	Specimen 1	1020.3	1379.1	15.0
	Specimen 3	929.3	1298.8	13.3

Table 3
Hardness profiles in function of the distance from the stud axis.

Distance from centre [mm]	HB (A)	HB (B)
0	381.4	
10	390.2	387.2
20	395.1	396.1
30	403.7	406.9
40	424.6	402.2

4. Discussion and conclusions

The broken stud featured an extensive network of cavities at the fracture surface and in the adjacent volumes on top and bottom sides of the fracture, identified by UT and further confirmed by metallographic observations. These cavities were located mainly towards the inner diameter where also the initiation was identified. In the volume of the broken stud close to the rupture, results of tensile tests confirmed that the certified tensile properties were not fulfilled for any of the specimens. In particular, the specimens extracted from the inner position featured a very limited ductility. When observing the initiation site of their fragile tensile breakdown reproducing at a local scale the rupture of the stud featuring almost total absence of ductility, this coincides with a cavity or network of cavities. Based on the investigations performed, the delayed rupture of the stud is compatible with a failure under sustained tensile stress, initiating from a central position featuring very poor ductility, moreover severely weakened by the presence of a large network of cavities not closed by the forging operations. After an initiation time, the subsequent fast propagation through the extensive continuous network of intergranular δ and Laves phases resulted in an overall brittle rupture with almost absent local necking. Even under a preloading stress lower than nominal, after a delay time the product was not forgiving due to the combined effect of an improper steel remelting, resulting in ingots affected by cavities that an insufficient forging reduction did not allow to close, and a non-optimised combination of composition and applied thermal treatment. This resulted in a continuous network of secondary phases embrittling the GB and inducing a local lack of ductility, poor tensile strength and impact toughness. In order to exclude the simultaneous occurrence of cavities and embrittling phases, UT procedures were developed to confirm that the remaining bolts, including the installed ones, are free of cavities using sufficiently conservative criteria [4]. In particular, in-situ axial inspections allowed installed bolts that could contain relevant imperfections to be identified and replaced. Fatigue crack propagation behaviour is suggested to be considered for future work.

Declaration of Competing Interest

The authors declare that they have no known competing financial interests or personal relationships that could have appeared to influence the work reported in this paper.

Data availability

No data was used for the research described in the article.

Acknowledgments

Thanks are owed to NHFML (R. Walsh) for performing the fracture toughness tests, to the company Linde AG for the impact toughness results and to Evans Analytical Group for the gas content assessment, as well as to the supplying company for extensive discussions all along the failure analysis process.

"The views and opinions expressed herein do not necessarily reflect those of the ITER Organization"

References

[1] P.Y. Lee, et al., Design, qualification & manufacture of ITER gravity supports, Heliyon 6 (2020), https://doi.org/10.1016/j.heliyon.2020.e03609.
[2] P. Shailesh, et al., Superalloy 718: evolution of the alloy from high to low temperature application, in: Proceedings of the 9th international symposium on superalloy 718 & derivatives: Energy, aerospace, and industrial applications. Springer, Cham, 2018.
[3] Edited by R.J. Siddall, Comparison of the Attributes of VIM+ESR and VlM+VAR Alloy 718, in: Edward A. Loria (Ed.), Superalloys 718, 625 and Various Derivatives, 1991. Edited byThe Minerals, Metals & Materials Society.
[4] I.Aviles Santillana et al., "Advanced ultrasonic examination of heavy–gauge high strength studs for the ITER gravity supports", this conference and proceedings.
[5] Metals Handbook: Fractography and Atlas of Fractographs, 8th Edition, Volume 9, American Society for Metals, 1974, p. 228.
[6] J. Schirra, et al., Superalloys (1991) 375–388, https://doi.org/10.7449/1991/SUPERALLOYS_1991_375_388.
[7] H.R. Gray, "Embrittlement of nickel-, cobalt-, and iron-base superalloys by exposure to hydrogen", NASA Technical Note TN d-7805 (1975).
[8] P.D. Hicks, C.J. Altstetter, Metall. Mater. Trans. A 21 (1990) 365–372, https://doi.org/10.1007/BF02782416.
[9] Y. Haruna, "Removal of inclusions from cast superalloy revert." (1994), University of British Columbia MSc. Thesis.